Polymer 55 (2014) 602–610

Contents lists available at ScienceDirect

Polymer

journal homepage: www.elsevier.com/locate/polymer

# Self-assembly behavior of rod–coil–rod polypeptide block copolymers

Zeliang Zhuang, Chunhua Cai, Tao Jiang, Jiaping Lin*, Chaoying Yang

*Shanghai Key Laboratory of Advanced Polymeric Materials, Key Laboratory for Ultrafine Materials of Ministry of Education, School of Materials Science and Engineering, East China University of Science and Technology, Shanghai 200237, China*

ARTICLE INFO

*Article history:*
Received 30 August 2013
Received in revised form
2 December 2013
Accepted 7 December 2013
Available online 14 December 2013

*Keywords:*
Polypeptide
Self-assembly
Rod–coil block copolymer

ABSTRACT

Self-assembly behavior of rod–coil–rod poly(γ-benzyl-L-glutamate)-*b*-poly(ethylene glycol)-*b*-poly(γ-benzyl-L-glutamate) (PBLG-*b*-PEG-*b*-PBLG) triblock copolymers with various PBLG block lengths in aqueous solution was investigated. The PBLG-*b*-PEG-*b*-PBLG triblock copolymers are able to self-assemble into vesicles when PBLG block length is relatively short. Meanwhile, the initial polymer concentration was found to have influence on the self-assembly. Giant vesicles can be observed when the initial concentration is high. Dissipative particle dynamics (DPD) simulations about the vesicles revealed that the rigid rod blocks could be aligned parallelly with each other to form the monolayer vesicles wall. When the PBLG block length in the PBLG-*b*-PEG-*b*-PBLG triblock copolymers increases, the aggregate morphologies were observed to transform from vesicles to spherical micelles. Based on the experimental and simulation results, we proposed a possible mechanism of the morphological transitions of the rod–coil–rod triblock copolymer aggregates.



## 1. Introduction

Amphiphilic block copolymers are able to self-assemble into various supramolecular aggregates in selective solvents. Diversiform morphologies such as spheres, rods, vesicles, spindles, tubules, toroids, and other complex structures have been observed [1–5]. These structures have attracted widespread interest for their potential applications in drug delivery systems, coatings, cosmetics, and nanoreactors [6–9]. In the past decade, many studies have been carried out on the self-assembly of coil–coil type amphiphilic block copolymers. For example, in a series of literature, Eisenberg et al. reported the self-assembly behavior of amphiphilic polystyrene-based block copolymers (*e.g.*, polystyrene-*b*-poly(acrylic acid) and polystyrene-*b*-poly(ethylene oxide)). They revealed that by adjusting the external conditions such as solvents, block length, pH value, and salt addition, the morphologies of aggregates can be well manipulated [10–12].

Rod–coil block copolymers, which consist of a rigid rod segment jointed to a flexible coil block, exhibit much more distinct self-assembly features because of the ordered packing mode of rigid blocks during aggregation and the additional interactions that can occur between anisotropic rod blocks [13–18]. Thus, rod–coil block copolymers are conceived to possibly have different self-assembly behavior from coil–coil ones [19–23]. Jenekhe's group reported that poly(phenylquinoline)-*b*-polystyrene (PPQ-*b*-PS) rod–coil block copolymers can self-assemble into diverse aggregates in organic solvents by tuning the PPQ rod block length or solvent quality. Among those aggregates, the vesicles have a specific single-layer structure owing to the dense and ordered packing of the π-conjugated PPQ rod blocks [22,23]. Self-assembly of these rod–coil block copolymers provides an opportunity to generate functional materials with well-defined supramolecular architectures and special properties. So far, self-assembly of rod–coil block copolymers with short rod block has been focused [13,24]. However, due to the limitation of synthesis technology and poor solubility of rod blocks in solvents, little attention was devoted to the self-assembly of rod-coil block copolymers with long rigid rod [14,19].

Recently, increasing attention has been paid to the polypeptide-based self-assemblies due to their biocompatibility and advantages in controlling both the functions and structures of the supramolecular aggregates [25–29]. Polypeptides can adopt well ordered secondary structure such as α-helix and β-sheet, as a result of the intra- and inter-molecular hydrogen bonds, respectively [29,30]. The α-helical structure is thought to give rise to a rigid-rod structure, which can be employed as a model rigid-rod polymeric system. The incorporation of polypeptide-based rigid chains and other synthetic coil chains is a particular valuable approach to creating novel supramolecular architectures [31–36]. For example, Chang

* Corresponding author. Tel.: +86 21 64253370.
*E-mail addresses:* jlin@ecust.edu.cn, jplinlab@online.sh.cn (J. Lin).

0032-3861/$ – see front matter © 2013 Elsevier Ltd. All rights reserved.
http://dx.doi.org/10.1016/j.polymer.2013.12.016

et al. studied the self-assembly behavior of poly(Z-L-lysine)-*block*-poly(*N*-isopropylacrylamide) (PZLys-*b*-PNIPAm) rod–coil block copolymers and found that these amphiphilic block copolymers are able to form vesicles in dilute solution, in which the rigid polypeptide chains take side by side packing mode to form the vesicle wall [35]. Our group reported the aggregation behavior of PBLG-*b*-PEG block copolymers in chloroform/ethanol/trifluoroacetic acid (TFA) mixed solution [36]. The micelles are formed with PEG as the shell and PBLG as the core. In the absence of TFA, PBLG adopts a rigid α-helix conformation, and the block copolymers self-assemble into cylindrical micelles. The polypeptide blocks within the cores are interdigitated and favor ordered parallel packing, with their long axis aligning in an orientation vector. The vector could gradually change along the long-center-axis of the micelle in a cholesteric liquid crystal manner. When the denaturant acid TFA is added, polypeptide chains become random coils. Spherical micelles with coiled polypeptide blocks randomly packing inside the cores are formed.

Generally, self-assembly of polypeptide-based rod–coil block copolymers with short rod block (or low volume fraction of rod block) has been well studied, and universal aggregate morphologies such as spherical micelles, cylindrical micelles, and vesicles were observed [29,31,35–39]. However, limited attention was focused on the self-assembly of the polypeptide block copolymers with long rod block (or high volume fraction of rod block). The underlying complex mechanism of the self-assembly of polypeptide-based copolymers with various lengths of polypeptide chain is still not clear enough.

In this work, we report the self-assembly behavior of rod–coil–rod poly(γ-benzyl-L-glutamate)-*b*-poly(ethylene glycol)-*b*-poly(γ-benzyl-L-glutamate) (PBLG-*b*-PEG-*b*-PBLG) triblock copolymers with various rigid PBLG block lengths. It was found that the PBLG-*b*-PEG-*b*-PBLG triblock copolymers containing relatively short PBLG block length can self-assemble into vesicles, and giant vesicles can be obtained at high initial concentrations. Moreover, dissipative particle dynamics (DPD) simulations about the vesicles revealed that the rigid rod blocks are aligned parallelly with each other to form the monolayer vesicle wall. Interestingly, with increasing the PBLG block length, the aggregate morphologies transform from vesicles to spherical micelles. By combining experimental findings with DPD results, a possible mechanism of the morphological transitions of the rod–coil–rod triblock copolymer aggregates is suggested.

## 2. Experimental section

### 2.1. Materials

α,ω-Diamino-poly(ethylene glycol) ($NH_2$–PEG–$NH_2$) ($M_w$ = 2000) was purchased from Sigma Inc. Analytical grade of hexane, tetrahydrofuran (THF), and 1,4-dioxane were refluxed with sodium and distilled immediately before use. All the other reagents are of analytical grade and used as received. The dialysis bag (Membra-cel, 3500 molecular weight cutoff) was provided by Serva Electrophoresis GmbH.

### 2.2. Synthesis of PBLG-b-PEG-b-PBLG triblock copolymers

Poly(γ-benzyl-L-glutamate)-*block*-poly(ethylene glycol)-*block*-poly(γ-benzyl-L-glutamate) triblock copolymers (PBLG-*b*-PEG-*b*-PBLG, abbreviated as BEB) were synthesized by ring-opening polymerization of γ-benzyl-L-glutamate-N-carboxyanhydride (BLG-NCA) initiated by $NH_2$–PEG–$NH_2$ with 1,4-dioxane as solvent [40,41]. After reacted at room temperature for 3 days, the viscous reaction mixture was poured into a large volume of anhydrous ethanol. The precipitated product was dried under vacuum and then purified twice by repeated precipitation from a chloroform solution into a large volume of anhydrous methanol. Finally, the product was dried under vacuum and white power was collected.

### 2.3. Synthesis of P(BLG-co-ELG)-b-PEG-b-P(BLG-co-ELG) block-random copolymers

Poly((γ-benzyl-*co*-γ-ethyl)-L-glutamate)-*block*-poly(ethylene glycol)-*block*-poly((γ-benzyl-*co*-γ-ethyl)-L-glutamate) block-random copolymers (P(BLG-*co*-ELG)-*b*-PEG-*b*-P(BLG-*co*-ELG), abbreviated as BEB-Et) were prepared by ester exchange reaction of BEB triblock copolymer with ethanol [42,43]. The reaction was performed at 55 °C in 1,2-dichloroethane (DCE) with *p*-toluenesfulfuric acid (TSA) as a catalyst. Then the reaction mixture was precipitated into a large volume of anhydrous methanol. The product was purified twice by repeated precipitation from a chloroform solution into a large volume of anhydrous methanol and then dried under vacuum. By the variation of molar ratio of BLG unit to ethanol and the reaction time, the degree of substitution of ethyl group (ratio of number of ELG unit to total number of BLG and ELG units) can be adjusted.

### 2.4. Preparation of micelles

The polymeric micelle solutions were prepared by using a dialysis method. First, the BEB triblock copolymers were dissolved in THF by stirring at room temperature for 2 days to obtain stock solutions with various initial polymer concentrations. To prepare micelle solution, 5 mL of deionized water, a selective solvent for PEG, was added to 10 mL of polymer solution at a rate of 0.01 mL/s with vigorous stirring. Subsequently, all the solution was dialyzed against deionized water for 3 days to ensure that all the organic solvents were removed. Before analysis, the solutions were stabilized for at least 5 days.

### 2.5. $^1H$ NMR

The composition of all copolymers was determined by $^1H$ NMR spectrum (Avance 550, Bruker) using deuterated chloroform ($CDCl_3$) with 15 vol% deuterated trifluoroacetic acid (TFA-d) as solvent and tetramethylsilane (TMS) as an internal standard.

### 2.6. Gel permeation chromatography

The polydispersity index of BEB triblock copolymers was determined by gel permeation chromatography (GPC, Varian, PL GPC-50 plus). A 20 mM LiBr/DMF solution was used as the mobile phase at the flow rate of 0.8 mL/min ($T$ = 49 °C). The calibration curve was obtained by narrow polydispersity PS standards.

### 2.7. Circular dichroism (CD)

CD analyses of the polypeptides were performed with a Chirascan spectrometer at room temperature. The diluted solutions (0.01 mg/mL) were introduced in quartz cells with 1 cm optical path length. Wavelengths between 190 and 300 nm were analyzed, with an integration time of 0.5 s and a wavelength step of 1 nm.

### 2.8. Fourier transform infrared spectrum (FTIR)

FTIR spectra of the samples were recorded on a Nicolet 5700 FTIR spectrometer at frequencies ranging from 400 to 4000 $cm^{-1}$. The sample powers were thoroughly mixed with KBr and pressed into pellet form. The tests were performed at room temperature.

### 2.9. Turbidity measurements (OD)

Turbidity measurements were performed to determine the critical water content for the aggregate formation. The BEB triblock copolymer was first dissolved in THF with a concentration of 0.5 g $L^{-1}$. Deionized water was then added drop by drop (0.02 mL per drop to 2 mL of polymer solution) with vigorous stirring. And after each drop of deionized water was added, the solution was stirred for 1 min and then left to equilibrate for 2 min or more until the optical density was stable. The optical density (turbidity) was measured at a wavelength of 500 nm (which was far from the absorption of the benzene chromophore) using a quartz cell (path length: 1 cm) with a UV–Vis spectrophotometer (UV–Vis UV-2550 SHIMADZU).

### 2.10. Transmission electron microscopy (TEM)

The morphologies of aggregates were examined by TEM (JEM-2100F, JEOL) operated at an accelerating voltage of 200 kV. Drops of solution were placed on a copper grid coated with carbon film and then dried at room temperature.

### 2.11. Scanning electron microscopy (SEM)

The morphologies of aggregates were also observed by SEM (S4800, HITACHI) operated at an accelerating voltage of 15 kV. The samples were prepared by placing drops of solution on a copper grid coated with carbon film and then dried at room temperature. Before the observations, the samples were sputtered by Aurum.

### 2.12. Atom force microscopy (AFM)

AFM measurements were performed with XE-100 (Park Systems) by using the non-contact mode at room temperature in air. The samples were prepared by placing drops of solution on a fresh-cleaved mica surface and allowed to dry in air.

### 2.13. Laser light scattering measurements (LLS)

The structure of the aggregates was characterized by combining dynamic (DLS) and static light scattering (SLS) measurements, which were performed on a commercial LLS spectrometer (ALV/CGS-5022F) equipped with an ALV-High QE APD detector and an ALV-5000 digital correlator using a He–Ne laser (the wavelength $\lambda = 632.8$ nm) as light source. All the samples were filtered through 0.8 μm filters to remove dust before the light scattering measurements, and all the measurements were carried out at 20 °C. From DLS testing, hydrodynamic radius ($R_h$) can be obtained, which provides the radius of a hard sphere with the same translational diffusion coefficient and the same condition. While the SLS measurements give the radius of gyration ($R_g$), which reflects the density distribution of the chain in real physical space. The details of the LLS testing method are provided in the Supporting Information.

## 3. Results and discussion

### 3.1. Characterization of BEB triblock copolymer

The BEB triblock copolymers were characterized by $^1$H NMR and GPC. Fig. 1 shows the $^1$H NMR spectrum of the BEB triblock copolymer in $CDCl_3$ with 15 vol% TFA-d. Since the degree of polymerization (DP) of the PEG block is known (45), the molecular weight of PBLG block can be calculated by peak intensities of methylene proton signal (5.1 ppm) of PBLG and the methylene proton signal (3.6 ppm) of PEG in the $^1$H NMR spectrum. The polydispersity index of BEB triblock copolymers was determined by GPC. As representative samples, GPC traces of BEB80 (the "80" denotes the degree of polymerization of each PBLG block determined from $^1$H NMR) and BEB210 display a monomodal symmetric distribution, which indicates a well-controlled polymerization process (Fig. 2). The molecular characteristics of the BEB triblock copolymers were summarized in Table 1. In addition, the degree of substitution of ethyl group for BEB-Et were calculated by peak intensities of the methine proton signal (4.6 ppm) of polypeptide backbone and the methylene proton signal (4.2 ppm) of ethyl group in the $^1$H NMR spectrum (Shown in Fig. S1). The assignment of the peptide secondary structures can be further confirmed by CD and FTIR measurements [44–46]. The results indicate that both the BEB triblock copolymers and the BEB-Et copolymers adopt α-helical secondary structure in neutral solvents, as shown in Figs. S2–S3 (see the Supporting Information).

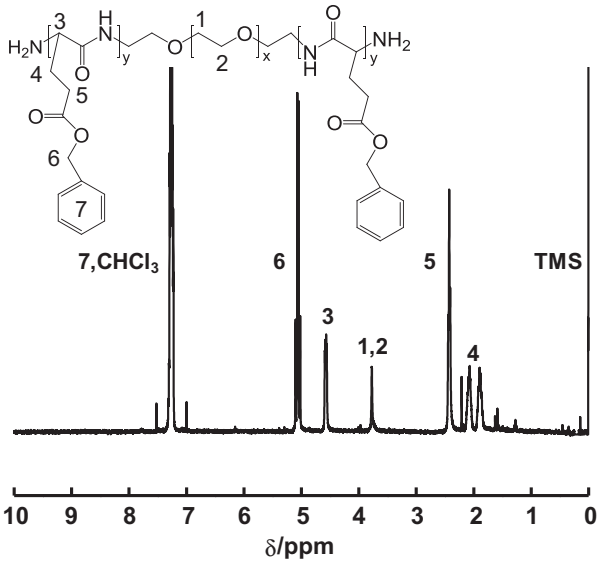


**Fig. 1.** $^1$H NMR spectrum of BEB triblock copolymers in $CDCl_3$ with 15 vol% TFA-d.

### 3.2. Effect of PBLG block length on self-assembly

When selective solvent, water, is added to BEB stock solution, the hydrophobic polypeptide blocks become insoluble and tend to form aggregate core outspreaded with hydrophilic PEG chains. Fig. 3 shows typical SEM images and hydrodynamic radius

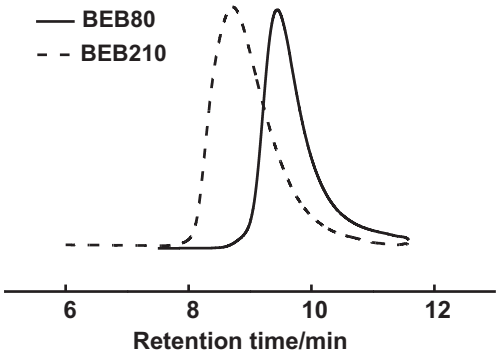


**Fig. 2.** GPC traces of BEB80 and BEB210 triblock copolymers.

**Table 1**
Characteristics of BEB triblock copolymers.

| Sample | $DP_{PBLG}$[a] | $M_n$[b] (g mol$^{-1}$) | $M_w/M_n$[c] |
|---|---|---|---|
| BEB80 | 80 | 37,040 | 1.18 |
| BEB110 | 110 | 50,180 | 1.23 |
| BEB150 | 150 | 67,700 | 1.25 |
| BEB210 | 210 | 93,980 | 1.15 |

[a] Degree of polymerization of one PBLG segment determined by $^1$H NMR in $CDCl_3$ with 15 vol% TFA-d.
[b] Number average molecular weight of BEB triblock copolymers, determined by $^1$H NMR in $CDCl_3$ with 15 vol% TFA-d.
[c] Determined by GPC.

distribution of aggregates self-assembled from BEB triblock copolymers with various PBLG block lengths, where the initial concentration is 0.5 g L$^{-1}$. For the BEB80 triblock copolymer, vesicles with a broad size distribution are observed (Fig. 3a). Most of them are broken and show flat form with raised area, due to the collapse and shrink of vesicles during the drying process. The inset plot of Fig. 3a shows a broad hydrodynamic radius distribution of vesicles and gives a mean hydrodynamic radius ($<R_h>$) value of 154.0 nm, which are well agreement with the SEM observation. The BEB110 can also self-assemble into vesicles with mean $<R_h>$ value of 127.3 nm (Fig. 3b). With increasing the PBLG block length (BEB150), interestingly, the aggregates transform from vesicles to spherical aggregates. The spherical aggregates with narrow distribution are much smaller than the vesicles, as shown in Fig. 3c. It can be noticed that the surfaces of spherical aggregates are collapsed slightly, indicating that the aggregates are not fully solid micelles in the aqueous solution. Upon further increasing PBLG block length, spherical solid aggregates are formed by BEB210 indicated by the smooth surface (Fig. 3d). The inset plot of Fig. 3d shows a narrow size distribution of aggregates and gives a mean $<R_h>$ value of 63.3 nm.

We have also carried out a control experiment in the preparation of the samples for SEM observations. In such an experiment, drops of micelle solution were frozen by liquid nitrogen, and then dried rapidly under vacuum to keep the aggregate morphology (frozen-dry method). The SEM images of BEB110 vesicles and BEB210 spherical micelles are shown in Fig. S4 (see the Supporting Information), which are similar to SEM images shown in Fig. 3. These results suggest that for present BEB systems, the drying process in the preparations does not affect the aggregate structures.

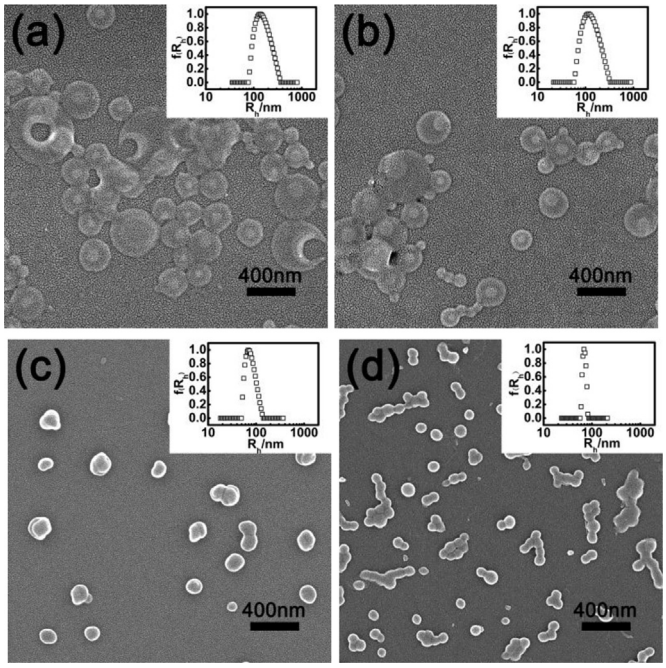


**Fig. 3.** Typical SEM images of aggregates formed by various triblock copolymers at the initial concentration of 0.5 g L$^{-1}$: (a) BEB80; (b) BEB110; (c) BEB150; and (d) BEB210. Inset plots are hydrodynamic radius distribution of aggregates in aqueous solution.

The aggregate morphologies were further examined by TEM and AFM analyses. Fig. 4a and b shows the typical TEM images of vesicles self-assembled from BEB80 and BEB110, respectively. The darker areas in the projection image of vesicles indicate the thickness of polymers in these areas is relatively high, which correspond to the raised areas of vesicles observed by SEM [11,47]. For the aggregates formed by BEB150 and BEB210, spherical shapes are displayed (Fig. 4c and d). Fig. 5 represents the AFM results for the vesicles. As can be seen, the AFM images of both BEB80 and BEB110 vesicles (Fig. 5a and b) display flat form with raised area and have broad size distributions. In addition, the height profiles of vesicles in Fig. 5a and b show the height of vesicle periphery is about 32 nm and 40 nm, respectively, which should be twice the thickness of vesicle wall [48]. Take BEB110 for example, as shown in Fig. 5b and c, it can be estimated that the thickness of vesicle wall is about 20 nm, which closes to the contour length of PBLG helical block (*ca.* 16.5 nm). These results indicate that the rigid PBLG blocks in vesicle wall are aligned parallelly with each other to form monolayer vesicle wall.

The proposed self-assembled structures as shown in Fig. 5c are further supported by a simulation study. We performed the DPD simulation of a rod–coil–rod triblock copolymer, whose structural parameters correspond to those of the experimental BEB80 sample. In the simulated copolymer, the rigid rod block consists of 8 bonded DPD particles with the block length $l_{Rod} = 4.9r_c$ ($r_c$ is cut-off radius). The repulsive parameters are set to produce strong segregation between hydrophobic rod block and solvent or hydrophilic coil block (The simulation details are shown in the Supporting Information). The spherical vesicle structure self-assembled from a $\mathbf{R_8C_4R_8}$ copolymer model is presented in Fig. 6. From the cross section of vesicle in Fig. 6b, it can be found that the rigid rod blocks are aligned parallelly with each other to form the vesicle wall. The external dimension of vesicle is estimated to be $19r_c$ (Fig. 6a), and the thickness of vesicle wall is about $6r_c$ (Fig. 6b). The thickness approaches to the rod block length, which validates again the formation of experimentally observed monolayer vesicle. Additionally, more detailed molecular information about the vesicles can be obtained via analyzing the density distributions of rod and coil blocks in vesicles. The density profiles are shown in Fig. 6c. The insert shows the two-dimensional section of the vesicle, and the origin of coordinates denotes the center of vesicle. The profile of R density ($\varphi_R$) displays a bimodal feature, while C density ($\varphi_C$) displays a tetramodal feature, which is a typical character of the vesicles.

The change of aggregate structure can also be viewed in terms of the ratio of average radius of gyration ($<R_g>$) to $<R_h>$ ($<R_g>/<R_h>$), which is sensitive to the particle shape [49,50]. Generally, $<R_g>/<R_h> = 0.774$ is regarded as a uniform and nondraining sphere. When $<R_g>/<R_h> = 1$, it can be attributed to a vesicle geometry in theory. For nonspherical structures, $<R_g>/<R_h>$ usually has a large value. The detailed LLS results of self-assembled aggregates of the BEB triblock copolymers are summarized in Table 2. One can see that the $<R_g>/<R_h>$ values of BEB80 vesicles and BEB110 vesicles are 1.08 and 1.09, respectively, which are very close to the ideal one. The $<R_g>/<R_h>$ values of aggregates formed by BEB150 and BEB210 are 0.87 and 0.84, respectively, which correspond to spherical structures. All these DLS results are well agreement with the observations from the microscopies.

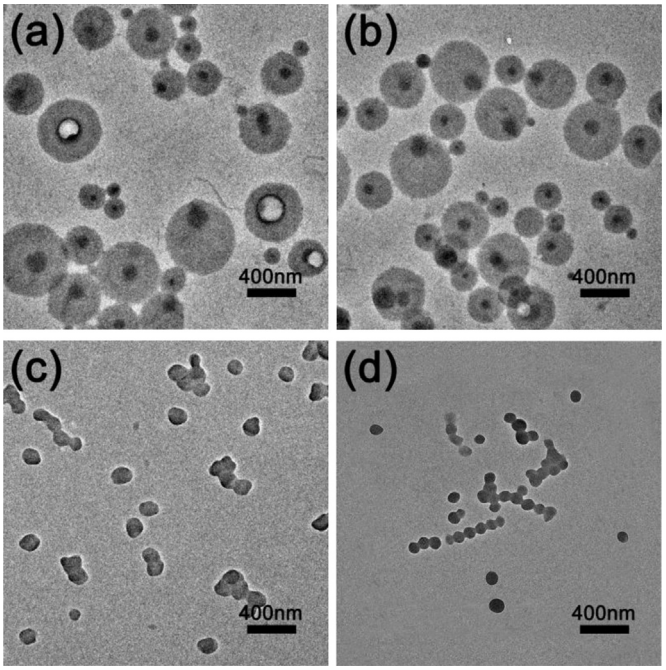


**Fig. 4.** Typical TEM images of aggregates formed by various triblock copolymers at the initial concentration of 0.5 g $L^{-1}$: (a) BEB80; (b) BEB110; (c) BEB150; and (d) BEB210.

### 3.3. Effect of initial concentration on self-assembly

The effect of initial concentration on aggregation behavior of BEB triblock copolymers was studied by SEM observation. Fig. 7 shows typical SEM images and hydrodynamic distribution of aggregates formed by BEB triblock copolymers at two different initial concentrations ($c = 0.1$ g $L^{-1}$, and 1.0 g $L^{-1}$). For BEB80, as shown in Fig. 7a, SEM image reveals that vesicles with a narrow size distribution can be obtained at the lower initial concentration ($c = 0.1$ g $L^{-1}$). When increasing the initial concentration, interestingly, giant vesicles with a broad size distribution are observed (Fig. 7b, $c = 1.0$ g $L^{-1}$). Meanwhile, for BEB110 vesicles, the effect of initial concentration on size and size distribution is similar to those of BEB80 triblock copolymer, as shown in Fig. 7c and d. As for the samples with longer PBLG block length (BEB150 and BEB210), spherical aggregates are obtained at the initial concentration of 0.1 g $L^{-1}$ (Fig. 7e and g), which have a narrow size distribution. When the initial concentration increases to 1.0 g $L^{-1}$, the aggregates remain their spherical shape, but the size and size distribution are slightly larger and broader than those of aggregates formed at $c = 0.1$ g $L^{-1}$, respectively, as shown in Fig. 7f and h. In addition, the aggregates formed by BEB system with various concentrations are also studied by TEM and LLS (Figs. S5 and S6, see the Supporting Information). These results indicate the initial concentration has a significant effect on the size of vesicles self-assembled from BEB80 and BEB110, but less marked influence on that of spherical aggregates formed by BEB150 and BEB210.

The giant monolayer vesicles are interesting findings of the present work. They could be employed as a model system of nature vesicles, and applied for delivery of therapeutics, and mimicking of living cell behavior [28,51–53]. Furthermore, we found that with increasing the PBLG block length, the aggregates formed by BEB triblock copolymers transform from vesicles to spherical micelles, which is distinctly different from the widely observed self-assembly behavior of coil–coil block copolymers. To deepen the understanding of the underlying mechanism of such morphology transition, the effect of added water content on the BEB aggregation process was further studied.

### 3.4. Effect of added water content on aggregation process

In the experiments, water was gradually added into the initial solution to examine the dynamic process of the aggregate formation. The critical water content (CWC) of BEB triblock copolymers, which is defined as water content at which micellization starts, can be determined by turbidity measurements [11]. Fig. 8 shows the diagrams of UV absorbance versus added water content at an initial polymer concentration of 0.5 g $L^{-1}$. When the water content is low (less than 10 wt%), the absorbance values are close to zero and negligible changes in the magnitude of absorption are observed. As the water content reaches to a certain value, the value of intensity increases dramatically, corresponding to the onset of aggregation. We designated the intersection point of the tangent to the curve at the inflection with the horizontal tangent through the points at low water contents of the curve as the critical water content (CWC). As can be seen, the CWC value of BEB80 is 19.3 wt%. With increasing the PBLG length, the CWC value decreases from 19.3 wt% to 14.3 wt % for BEB210, which suggests the increase of self-assembly tendency of BEB triblock copolymers.

The effect of added water content on the aggregation process of BEB triblock copolymers was also followed by SEM. To obtain the aggregate structures at certain water content, water was added to

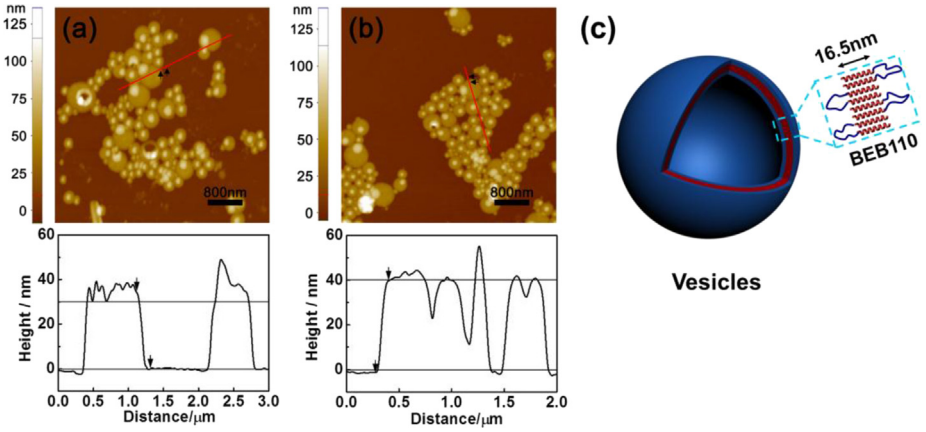


**Fig. 5.** Typical AFM images of vesicles formed by BEB triblock copolymers at the initial concentration of 0.5 g $L^{-1}$: (a) BEB80; (b) BEB110, and (c) Schematic representation of BEB vesicles.

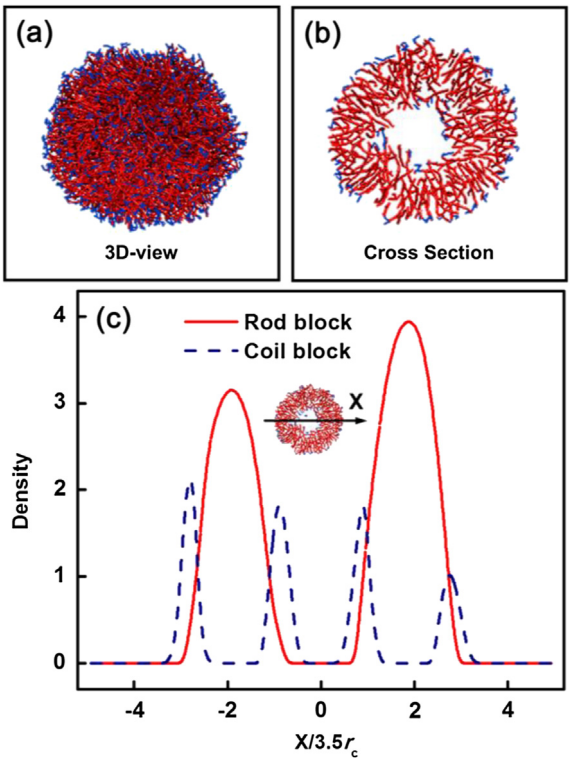


**Fig. 6.** DPD simulation snapshot of (a) vesicle structure from rod–coil–rod triblock copolymer, and (b) a cross section of vesicles. (c) One-dimensional density profiles along x-arrow of rod and coil blocks for the vesicle.

polymer solution to reach predetermined water content, and then the mixture solution was fast added to an amount of water to freeze the aggregate morphologies [3,54]. As shown in Fig. 9a–c, for BEB110, SEM images reveal that with the addition of water, BEB110 first self-assemble into spherical primary aggregates with diameter of about 80 nm (Fig. 9a), and then gradually transforms into vesicles (Fig. 9b). When the added water content reaches 25.1 wt%, vesicles with average diameter of 200 nm are clearly observed (Fig. 9c). For BEB210, the grain shape aggregates with about 50 nm in length and about 25 nm in width are obtained at the added water content of 14.7 wt% (Fig. 9d). With increasing water content, the aggregates transform to spherical micelles and the size of aggregates also simultaneously increases, as shown in Fig. 9e and f.

These results indicate that when the added water content reaches CWC value, primary aggregates of BEB triblock copolymers are formed. With increasing the water content, the primary aggregates can further evolve to larger aggregates to lower the system energy. For BEB triblock copolymers with relatively long PBLG length, forming larger spheres is fundamental favorable, since the longer block can pack in the hydrophobic cores densely with the junctions of rod and coil blocks anchored to hydrophobic/hydrophilic interfaces [55]. However, for BEB triblock copolymers with relatively short PBLG length, they do not support the formation of larger solid spheres with the rod/coil chain junctions anchored to hydrophobic/hydrophilic interfaces [22]. Instead, vesicles are formed to make the hydrophobic rods densely packed.

**Table 2**
Typical LLS results of self-assembled aggregates of BEB triblock copolymers.

| Sample[a] | $<R_h>$/nm | $<R_g>$/nm | $<R_g>/<R_h>$ | PDI[b] |
|---|---|---|---|---|
| BEB80 | 154.0 | 166.3 | 1.08 | 0.15 |
| BEB110 | 127.3 | 138.8 | 1.09 | 0.11 |
| BEB150 | 90.0 | 78.3 | 0.87 | 0.03 |
| BEB210 | 63.3 | 53.2 | 0.84 | 0.01 |

[a] The initial concentration of triblock copolymers is 0.5 g $L^{-1}$.
[b] Polydispersity index (PDI) of the aggregates is determined at the angle of 90°.

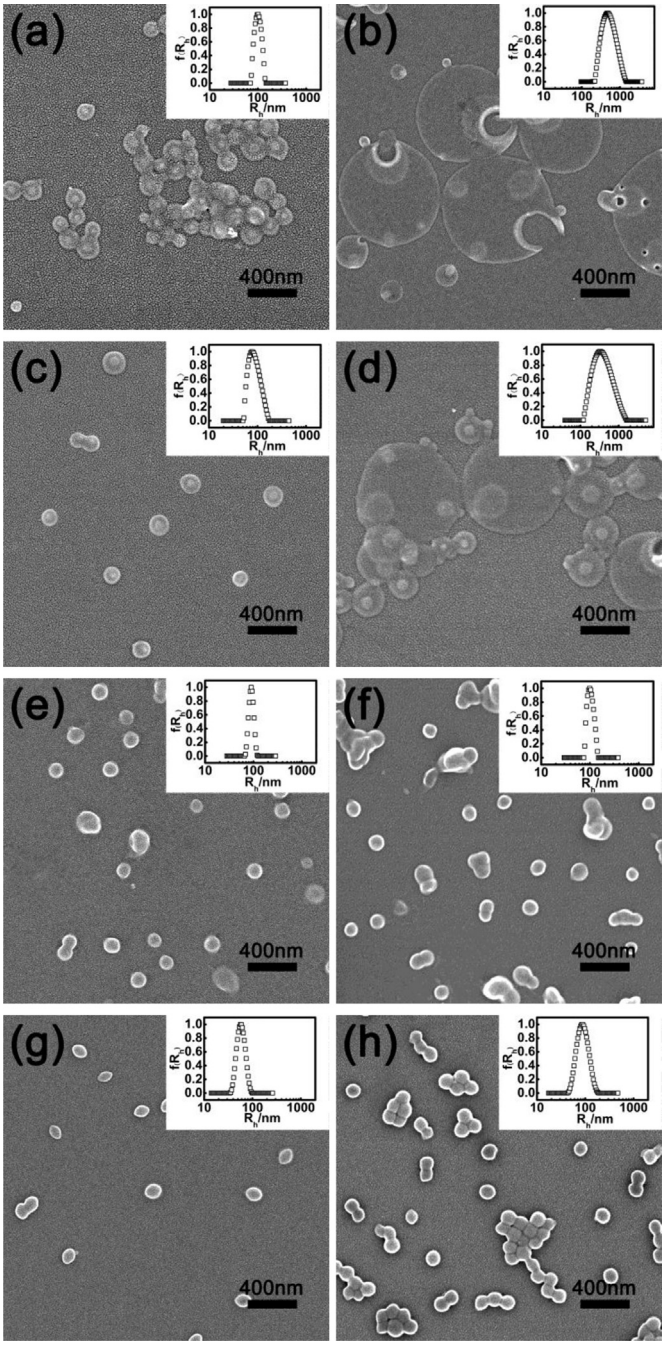


**Fig. 7.** Typical SEM images of aggregates formed by BEB triblock copolymers with various initial concentrations: (a) 0.1, and (b) 1.0 g $L^{-1}$ for BEB80; (c) 0.1, and (d) 1.0 g $L^{-1}$ for BEB110; (e) 0.1, and (f) 1.0 g $L^{-1}$ for BEB150; and (g) 0.1, and (h) 1.0 g $L^{-1}$ for BEB210. Inset plots are hydrodynamic radius distribution of aggregates in aqueous solution.

### 3.5. *Effect of interaction between PBLG blocks on self-assembly*

As be pointed out above, the self-assembly behavior of the triblock copolymers is thermodynamic controlled. However, when the water content is relatively higher, the further morphology

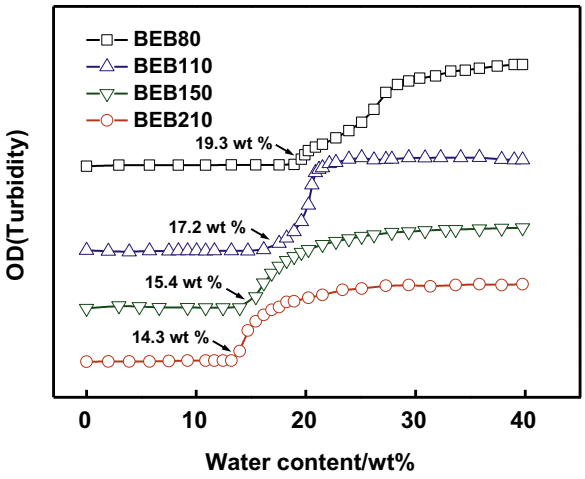


**Fig. 8.** Turbidity (optical density) curves of BEB triblock copolymer solution in THF at the initial concentration of 0.5 g $L^{-1}$ as a function of the amount of water added to the solution. The turbidity values for concentration in water smaller than 10 wt% are close to zero for all samples. The curves of BEB80, BEB110, and BEB150 are shifted for clarity.

transition is hindered due to the restriction of PBLG chains by poor solubility in the solvents. In addition to the solvophobic effect induced PBLG chain aggregation, the interchain attraction, due to the strong dipolar π–π interaction between the phenyl groups of PBLG blocks, could also contribute to the ordered packing of PBLG chains, which influences considerably the self-association [32,56–58]. Thus, it can be deduced that if the attraction between hydrophobic PBLG chains decreases, the mobility of PBLG chains can be retained at a relatively higher water content, which can induce the triblock copolymers further self-assemble into aggregates with much lower free energy. By substituting phenyl group in the PBLG side chain with ethyl group or introducing nanoparticles, the attraction between polypeptide chains is decreased and the mobility of PBLG chains increases. As a result, the morphological

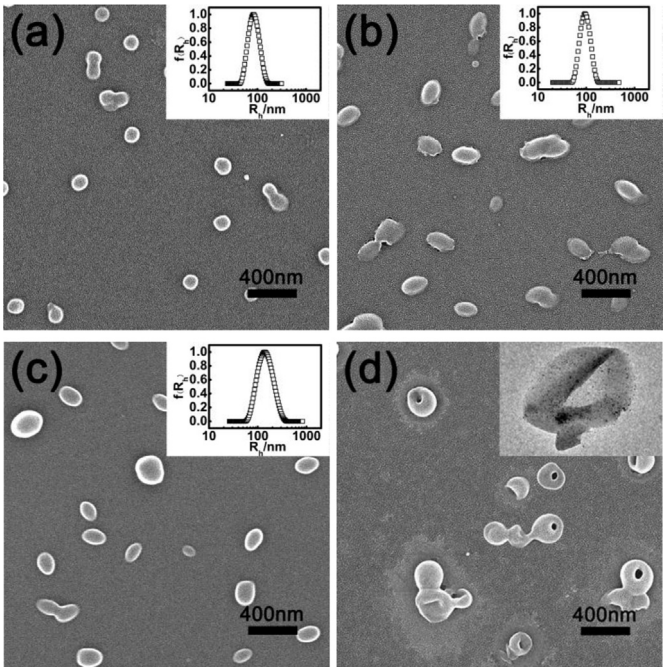


**Fig. 10.** Typical SEM images of aggregates formed by BEB210-Et with various degree of substitution of ethyl group: (a) 0.55, (b) 0.79, and (c) 0.91 at the initial concentration of 0.5 g $L^{-1}$. Inset plots are hydrodynamic radius distribution of aggregates in aqueous solution. (d) SEM image of vesicles formed by BEB210/AuNPs mixtures. Insert is TEM image of vesicles.

transitions of BEB system from large sphere to cylinders or vesicles can be observed.

By substituting phenyl groups with ethyl groups, the attraction between polypeptide chains is weakened due to the decrease of dipolar π–π interaction between polypeptide blocks. The BEB-Et block-random hydrophobic blocks reserve α-helical secondary

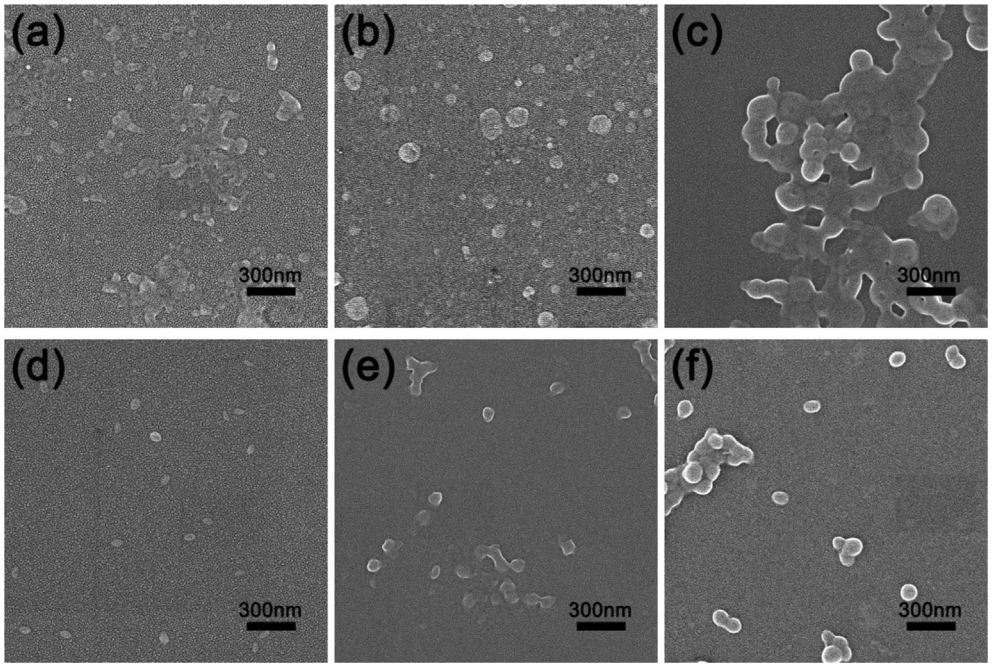


**Fig. 9.** TEM images of the aggregates self-assembled from BEB triblock copolymers (initial concentration of 0.5 g $L^{-1}$) with various added water content: (a) 17.6 wt%, (b) 20.2 wt%, and (c) 25.1 wt% for BEB110; (d) 14.7 wt%, (e) 16.9 wt%, and (f) 20.2 wt% for BEB210.

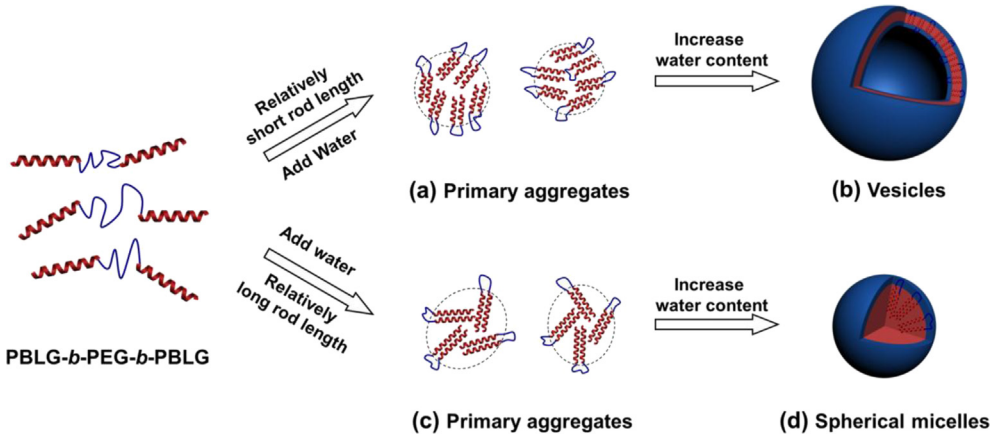


**Scheme 1.** Schematic representation of the morphological transitions of BEB triblock copolymers.

structure (see the Supporting Information, Figs. S2 and S3). As shown in Fig. 10a–c, typical SEM images and hydrodynamic distribution of aggregates formed by BEB210-Et with various degrees of substitution of ethyl group are displayed. For BEB210-Et1 with degree of substitution of 0.55, spherical micelles with mean $<R_h>$ value of 84.1 nm are obtained, which is similar to that of BEB210 (Figs. 10a and 3d). Interestingly, when the degree of substitution increases to 0.79, the aggregate morphologies transform to cylindrical micelles ($<R_h> = 94.5$ nm, Fig. 10b). With further increasing the degree of substitution, the size of the cylinders significant increases and size distribution becomes broader, as shown in Fig. 10c ($<R_h> = 142.3$ nm). In addition, the TEM images and the detailed DLS results of the aggregates formed by BEB210-Et are displayed in Fig. S7 and Table S1, respectively (see the Supporting Information).

As revealed by some recent work [59–61], the interchain attraction of PBLG rod blocks can be weakened by introducing nanoparticles, because the nanoparticles can break the ordered packing, thus weaken the interaction between the PBLG rods. Herein, hydrophobic 1-dodecanethiol-stabilized AuNPs with diameter of 7 nm were used to mix with BEB210 (ratio of weight of AuNPs to total weight of BEB210 and AuNPs is 0.05; for detailed information regarding the nanoparticles, see Supporting Information). As shown in Fig. 10d, the SEM image reveals that vesicles are obtained from BEB210/AuNPs mixtures. The distribution of AuNPs in the vesicles can be observed by TEM (insert of Fig. 10d). It shows that the AuNPs are located in the vesicle wall. These results suggest that the weakening of interchain attraction of PBLG rods by AuNPs has significant effect on the aggregation of BEB triblock copolymers, leading to the aggregate morphological transition from spherical micelles to vesicles.

### 3.6. Mechanism of self-assembly of BEB triblock copolymers

Based on the experimental results, a mechanism for the self-assembly of BEB triblock copolymers in aqueous solution was proposed. Scheme 1 shows a schematic illustration of morphological evolution of the BEB triblock copolymers. For BEB80 and BEB110 with relatively short PBLG blocks, when water is added, the hydrophobic PBLG chains tend to aggregate to form loose primary aggregates, in which the rigid PBLG chains could be not fully packed in order (Scheme 1a) [12,19]. With increasing the water, the aggregation number can further increases, resulting in an increase in interfacial energy of PBLG and PEG chains. In order to reduce this energy, the primary aggregates transforming to vesicles. It also has been proven by both experiments and DPD simulations that in the vesicle wall, the rigid PBLG chains are aligned parallelly with each other to form the monolayer vesicle wall (Figs. 5 and 6 and Scheme 1b). In addition, the proposed vesicles formation of BEB triblock copolymers was further supported by DPD simulations. The dynamics pathways of vesicles formation of $\mathbf{R}_8\mathbf{C}_4\mathbf{R}_8$ triblock copolymer model show that the triblock copolymers first form primary aggregates rapidly. Then, with increasing the self-assembly time, the primary aggregates get close and further fuse to form a disk-like membrane. Finally, the bending of membrane leads to the formation of a closed vesicle structure (see the Supporting Information, Fig. S9).

For BEB triblock copolymers with relatively long PBLG blocks (BEB150 and BEB210), with increasing the water content, the large spheres are formed (Scheme 1d). Within the large spheres, the longer block can pack in the hydrophobic cores densely with the junctions of rod and coil blocks anchored to hydrophobic/hydrophilic interfaces. A morphological transition from the large spheres to cylinders or vesicles (Fig. 10) can be observed by decreasing the interaction between polypeptide chains (substituting phenyl groups with ethyl groups or introducing nanoparticles to BEB system). In a word, from the results and discussion above, we learned that the interaction between rigid PBLG blocks is an important factor in the self-assembly of BEB triblock copolymers.

The self-assembly mechanism of amphiphilic coil–coil block copolymers has been well studied. However, it is not enough for the cognition about self-assembly of rod–coil block copolymers, which can exhibit much more distinct self-assembly features because of the ordered packing mode of rod blocks. In the present work, the aggregation behavior of rod–coil–rod polypeptide block copolymer with various lengths of rod block was examined. Such block copolymers exhibit special self-assembly behavior, *i.e.* the aggregates transform from vesicles to spherical micelles with increasing the hydrophobic PBLG length, in which the interaction between PBLG chains plays an important role in the self-assembly process. Studies on the self-assembly of such system can deepen our understanding about self-assembly of rod–coil block copolymers. Meanwhile, with this knowledge of aggregation of rod–coil polypeptide block copolymers, self-assembly structures with controllable shape and size can be more conveniently obtained by adjusting the external condition, which can facilitate their practical applications in such as intelligent drug delivery systems.

## 4. Conclusions

The self-assembly behavior of rod–coil–rod PBLG-*b*-PEG-*b*-PBLG (BEB) triblock copolymers was studied. It was found that BEB triblock copolymers with relatively short PBLG block (BEB80 and

BEB110) self-assemble into monolayer vesicles (at high initial concentration, giant vesicles can be obtained). With increasing the PBLG block length (BEB150 and BEB210), the aggregates transform from vesicles to spherical aggregates. It is believed that interaction between rigid PBLG blocks plays a key role in the self-assembly behavior of BEB triblock copolymer. When the interaction between PBLG blocks is relatively weak, the BEB triblock copolymers are prior to forming vesicles. However, as the interaction become stronger, the aggregate structures can be quickly frozen at the lower water content, which prevents the fusion of primary aggregates to more complex structures (cylinders and vesicles). This study enriched our knowledge in the self-assembly of triblock copolymer containing rigid polypeptide blocks and may provide useful guidance for designing polypeptide-based vesicles (giant vesicles) with controllable size, which could be potential applications in biomedical systems.

## Acknowledgment

This work was supported by National Natural Science Foundation of China (21234002, 50925308), Key Grant Project of Ministry of Education (313020) and National Basic Research Program of China (No. 2012CB933600). Support from projects of Shanghai municipality (10GG15 and 12ZR1442500) and Fundamental Research Funds for the Central Universities (WD1214008) are also appreciated.

## Appendix A. Supplementary data

Supplementary data related to this article can be found online at http://dx.doi.org/10.1016/j.polymer.2013.12.016.

## References

[1] Jain S, Bates FS. Science 2003;300(5618):460–4.
[2] Gerard R. Prog Polym Sci 2003;28(7):1107–70.
[3] Bhargava P, Tu Y, Zheng JX, Xiong H, Quirk RP, Cheng SZD. J Am Chem Soc 2007;129(5):1113–21.
[4] Wang X, Guerin G, Wang H, Wang Y, Manners I, Winnik MA. Science 2007;317(5838):644–7.
[5] Hadjichristidis N, Iatrou H, Pitsikalis M, Pispas S, Avgeropoulos A. Prog Polym Sci 2005;30(7):725–82.
[6] Liu J, Huang W, Pang Y, Zhu X, Zhou Y, Yan D. Biomaterials 2010;31(21):5643–51.
[7] van Dongen S, de Hoog H, Peters R, Nallani M, Nolte R, van Hest J. Chem Rev 2009;109(11):6212–74.
[8] Deming TJ. Prog Polym Sci 2007;32(8–9):858–75.
[9] Dash BC, Mahor S, Carroll O, Mathew A, Wang W, Woodhouse KA, et al. J Control Release 2011;152(3):382–92.
[10] Zhang L, Eisenberg A. J Am Chem Soc 1996;118(13):3168–81.
[11] Yu Y, Zhang L, Eisenberg A. Macromolecules 1998;31(4):1144–54.
[12] Zhang L, Eisenberg A. Polym Adv Technol 1998;9(10):677–99.
[13] Lee M, Cho BK, Zin WC. Chem Rev 2001;101(12):3869–92.
[14] Liu C, Lin C, Kuo C, Lin S, Chen W. Prog Polym Sci 2011;36(5):603–37.
[15] Cheng C, Huang Y, Tang R, Chen E, Xi F. Macromolecules 2005;38(8):3044–7.
[16] Rahman MS, Samal S, Lee JS. Macromolecules 2006;39(15):5009–14.
[17] Changez M, Kang NG, Koh HD, Lee JS. Langmuir 2010;26(12):9981–5.
[18] Yassar A, Miozzo L, Gironda R, Horowitz G. Prog Polym Sci 2013;38(5):791–844.
[19] Olsen BD, Segalman RA. Mat Sci Eng R 2008;62(2):37–66.
[20] Lin W, Zhang J, Wan X, Liang D, Zhou Q. Macromolecules 2009;42(12):4090–8.
[21] Cornelissen JJLM, Fischer M, Sommerdijk NAJM, Nolte RJM. Science 1998;280(5368):1427–30.
[22] Jenekhe SA, Chen XL. Science 1999;283(5400):372–5.
[23] Jenekhe SA, Chen XL. Science 1998;279(5358):1903–7.
[24] Tung YC, Wu WC, Chen WC. Macromol Rapid Comm 2006;27(21):1838–44.
[25] Rodriguez-Hernandez J, Lecommandoux S. J Am Chem Soc 2005;127(7):2026–7.
[26] Lin J, Zhu J, Chen T, Lin S, Cai C, Zhang L, et al. Biomaterials 2009;30(1):108–17.
[27] Cai C, Zhang L, Lin J, Wang L. J Phys Chem B 2008;112(40):12666–73.
[28] He C, Zhuang X, Tang Z, Tian H, Chen X. Adv Healthc Mater 2012;1(1):48–78.
[29] Carlsen A, Lecommandoux S. Opin Colloid Interface Sci 2009;14(5):329–39.
[30] Idelson M. J Polym Sci Polym Lett Ed 1985;23(11):604.
[31] Cai C, Wang L, Lin J. Chem Commun 2011;47(40):11189–203.
[32] Kim KT, Park C, Vandermeulen GWM, Rider DA, Kim C, Winnik MA, et al. Angew Chem Int Ed 2005;44(48):7964–8.
[33] Cai C, Lin J, Chen T, Wang X, Lin S. Chem Commun 2009;19:2709–11.
[34] Cai C, Lin J, Chen T, Tian X. Langmuir 2010;26(4):2791–7.
[35] Huang CJ, Chang FC. Macromolecules 2008;41(19):7041–52.
[36] Ding W, Lin S, Lin J, Zhang L. J Phys Chem B 2008;112(3):776–83.
[37] Huang J, Bonduelle C, Thévenot J, Lecommandoux S, Heise A. J Am Chem Soc 2012;134(1):119–22.
[38] Schatz C, Louguet S, Le Meins JF, Lecommandoux S. Angew Chem Int Ed 2009;48(14):2572–5.
[39] Zhuang Z, Zhu X, Cai C, Lin J, Wang L. J Phys Chem B 2012;116(33):10125–34.
[40] Cai C, Zhu W, Chen T, Lin J, Tian X. J Polym Sci Part A Polym Chem 2009;47(22):5967–78.
[41] Blout ER, Karlson RH. J Am Chem Soc 1956;78(5):941–6.
[42] Inomata K, Ohara N, Shimizu H, Nose T. Polymer 1998;39(15):3379–86.
[43] Li T, Lin J, Chen T, Zhang S. Polymer 2006;47(13):4485–9.
[44] Floudas G, Papadopoulos P, Klok HA, Vandermeulen GWM, Rodriguez-Hernandez J. Macromolecules 2003;36(10):3673–83.
[45] Ferretti JA, Ninham BW. Macromolecules 1970;3(1):30–3.
[46] Cauchois O, Segura-Sanchez F, Ponchel G. Int J Pharm 2013;452(1–2):292–9.
[47] Yang M, Wang W, Yuan F, Zhang X, Li J, Liang F, et al. J Am Chem Soc 2005;127(43):15107–11.
[48] Kim H, Jeong SM, Park JW. J Am Chem Soc 2011;133(14):5206–9.
[49] Vagberg LJM, Cogan KA, Gast AP. Macromolecules 1991;24(7):1670–7.
[50] Wu C, Li M, Kwan SCM, Liu GJ. Macromolecules 1998;31(21):7553–4.
[51] Zhou Y, Yan D. Angew Chem Int Ed 2004;43(37):4896–9.
[52] Sun J, Chen X, Deng C, Yu H, Xie Z, Jing X. Langmuir 2007;23(16):8308–15.
[53] Holowka EP, Sun VZ, Kamei DT, Deming TJ. Nat Mater 2007;6(1):52–7.
[54] Bhargava P, Zheng J, Li P, Quirk RP, Harris FW, Cheng SZD. Macromolecules 2006;39(14):4880–8.
[55] Antonietti M, Förster S. Adv Mater 2003;15(16):1323–33.
[56] Uematsu I, Uematsu Y. Adv Polym Sci 1984;59:37–73.
[57] Minich EA, Nowak AP, Deming TJ, Pochan DJ. Polymer 2004;45(6):1951–7.
[58] Junnila S, Houbenov N, Hanski S, Iatrou H, Hirao A, Hadjichristidis N, et al. Macromolecules 2010;43(21):9071–6.
[59] Pinol R, Jia L, Gubellini F, Levy D, Albouy PA, Keller P, et al. Macromolecules 2007;40(16):5625–7.
[60] Cai C, Wang L, Lin J, Zhang X. Langmuir 2012;28(9):4515–24.
[61] Barmatov EB, Pebalk DA, Barmatova MV. Langmuir 2004;20(25):10868–71.